Biochemical and Biophysical Research Communications 432 (2013) 345–349

Contents lists available at SciVerse ScienceDirect

Biochemical and Biophysical Research Communications

journal homepage: www.elsevier.com/locate/ybbrc

Closed-looped *in situ* nano processing on a culturing cell using an inverted electron beam lithography system

Takayuki Hoshino *, Kunihiko Mabuchi

Graduate School of Information Science and Technology, The University of Tokyo, 7-3-1 Hongo, Bunkyo-ku, Tokyo 113-8656, Japan

ARTICLE INFO

Article history:
Received 16 January 2013
Available online 8 February 2013

Keywords:
Real-time
Virtual molecular display
Electron beam
Cell membrane
Molecular dynamics

ABSTRACT

The beam profile of an electron beam (EB) can be focused onto less than a nanometer spot and scanned over a wide field with extremely high speed sweeping. Thus, EB is employed for nano scale lithography in applied physics research studies and in fabrication of semiconductors. We applied a scanning EB as a control system for a living cell membrane which is representative of large scale complex systems containing nanometer size components. First, we designed the opposed co-axial dual optics containing inverted electron beam lithography (I-EBL) system and a fluorescent optical microscope. This system could provide *in situ* nano processing for a culturing living cell on a 100-nm-thick SiN nanomembrane, which was placed between the I-EBL and the fluorescent optical microscope. Then we demonstrated the EB-induced chemical direct nano processing for a culturing cell with hundreds of nanometer resolution and visualized real-time images of the scanning spot of the EB-induced luminescent emission and chemical processing using a high sensitive camera mounted on the optical microscope. We concluded that our closed-loop *in situ* nano processing would be able to provide a nanometer resolution display of virtual molecule environments to study functional changes of bio-molecule systems.

1. Introduction

Even low energy electron beams (EBs) can be focused to a beam profile that is fine enough to process nanometer scale patterns on millimeter-wide fields. Additionally, EBs can be scanned at extremely high speed sweeping because of the small mass of electrons. These advantages of the EBs have meant that EB lithography is used for nanofabrication [1]. Electrons hitting a substrate surface induce emissions of various energy electrons known as secondary, Auger, and back scattering electrons, as the primary electrons scatter in the substrate. These emissions induce a chemical reaction not only on the surface but also inside of the substrate, since some primary electrons can reach depths of nanometers to micrometers in the substrate material depending on their initial kinetic energies. Applications of these transmitted electron energies have included using the scanning EB to capture super resolution images of wet biological specimens through a SiN nanomembrane with transmitted electrons [2–4], back scattered electrons [5,6], and electron-induced luminescence [7,8].

The penetrating and transmitting energies of EBs have been demonstrated a capability for direct processing in wet [9] and living [10,11] environments. We reported the principle of EB direct patterning at a living cell membrane by passing the EB through a SiN nanomembrane, and our experimental results showed little damage to the living hepatocyte cell membrane after the EB irradiation [10], though this processing had just open-loop beam control. We were able to use the EB energy to control an electro-chemical and physicochemical reaction under culturing conditions; that is, the reaction was controlled by the electron acceleration voltage. The fast and fine processing by EBs provides an approach capable of analyzing dynamic reactions of biochemical and biophysical systems, if the EBs are controlled in real-time by feedback from synchronized imaging of biochemical and biophysical responses.

Thus, here we have proposed closed-looped *in situ* nano processing using EB lithography. Synchronized imaging to the EB lithography and real-time observation during the EB irradiation was used to visualize dynamics of the EB-induced reaction on a living cell. We designed the opposed co-axial dual optics that included an inverted EB lithography (I-EBL) system and a fluorescent optical microscope. This system provided *in situ* nano processing of a culturing living cell on a 100-nm-thick SiN nanomembrane, which was placed between the I-EBL and the fluorescent optical microscope. The EB-induced chemical direct nano processing was demonstrated at the culturing cell with hundreds of nanometer resolution, and real-time images of the scanning spot of the EB-induced luminescent emission and chemical processing were visualized with a high sensitivity camera mounted on the optical microscope. We concluded that our closed-looped *in situ* nano processing would be able to provide a nanometer resolution display of virtual molecule environments to allow study of the functional changes on bio-molecule systems.

* Corresponding author.
E-mail address: takayuki_hoshino@ipc.i.u-tokyo.ac.jp (T. Hoshino).

0006-291X/$ - see front matter © 2013 Elsevier Inc. All rights reserved.
http://dx.doi.org/10.1016/j.bbrc.2013.01.100

2. Materials and methods

2.1. Opposed co-axial dual optics for in situ nano processing

The EB optics (Mini-EOC, Apco Co.) was inverted and positioned under a 100-nm-thick SiN nanomembrane to directly irradiate electrons into an aqueous solution at atmospheric pressure (Fig. 1A). The electrons were emitted from a thermal field emission type cathode, and were accelerated up to 5 keV. The SiN nanomembrane was supported by a 250-μm wide Si open window frame (NT025C, NORCADA) and the membrane separated the vacuum chamber of the EB optics from the aqueous solution. A fluorescent microscope (IM-3, Nikon) was co-axially mounted opposite the EB optics. The 100× water immersion objective lens (NA = 1.1, Nikon), LED white light source (SOLA, Lumencor), and high sensitivity scientific CMOS camera (NEO sCMOS, Andor) were attached on the microscope real-time imaging observation of the EB-induced reaction under the culturing conditions. The cultivation medium was warmed to 35–37 °C using a lens heater (Lens Heater, Tech-alpha).

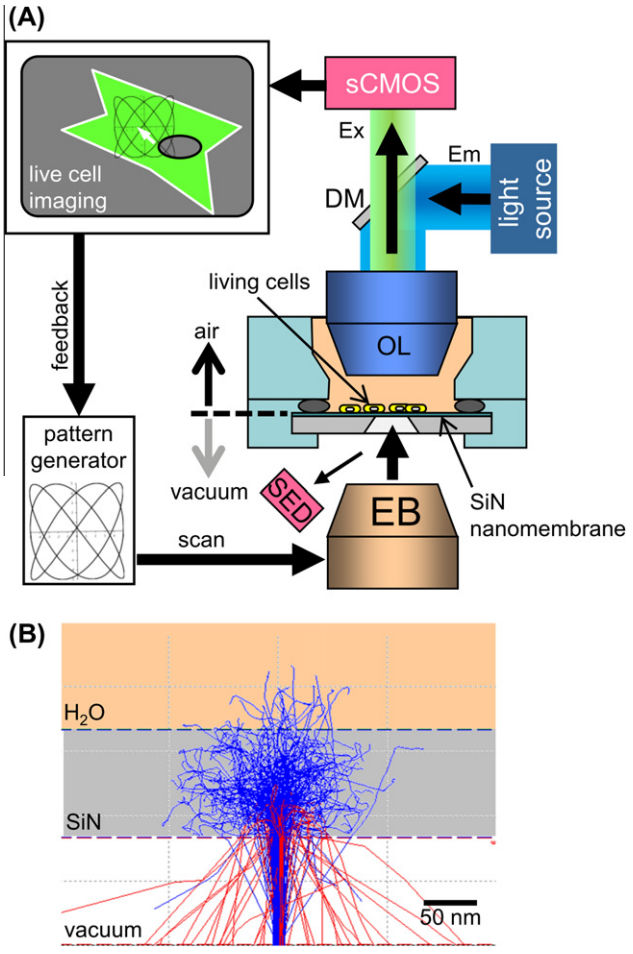

Fig. 1. Opposed co-axial dual optics of a fluorescent microscope and inverted electron beam lithography (I-EBL). (A) Schematic of the experimental setup. The I-EBL was mounted on the side opposite of a fluorescent microscope. A 100-nm-thick SiN nanomembrane was placed between the I-EBL and the fluorescent microscope to separate the atmospheric environment and the vacuum environment. The nanomembrane also worked as a cell culture surface and as a window for EB transmission. The high sensitivity sCMOS camera was synchronized to the EB scanning and provided real-time images as operating feedback. (B) Trajectories of scattered primary electrons and back scattered electrons by Monte Carlo simulation. The 10-nm-wide EB penetrated the 100-nm-thick SiN nanomembrane and the 0.1 MPa liquid H_2O layer from the lower side (vacuum side) of the SiN membrane.

Deflectors of the EB were connected to an *x*–*y* pattern generator to control the scanning pattern of the EB trajectory. The scanning data could be changed to the updated trajectory in real-time where the update was based on the real-time video images.

2.2. Simulation of the energy distribution of electrons

Trajectories of scattering electrons in the materials were simulated with the Monte Carlo simulator, CASINO ver. 2.42 [12]. Three layers consisting of a vacuum space, a 100-nm-thick SiN nanomembrane, and liquid H_2O were prepared, and a 10-nm-wide EB with 2.4–10 keV accelerating voltage was irradiated from the vacuum side of the layers. Energy profiles of transmitted electrons passing through the 100-nm-thick SiN nanomembrane and absorbed energy density at the interface between the SiN surface and H_2O, which were related to biological damage of molecules and to the chemical reaction, were simulated with various accelerating voltages.

2.3. Real-time observation of electron beam-induced luminescence and deposition

The beam deflector for the EB scanning was connected to the two-channel signal generator. The Lissajous diagram and rectangular raster scanning were inputted from the signal generator to the beam deflector. The scanning patterns on the SIN nanomembrane were captured with the sCMOS camera (pixel size = 6.5 × 6.5 μm) through the 100× objective lens (NA = 1.1). This camera was synchronized to the beam scanning to observe real-time images of the EB-induced reaction. EB-induced luminescence at the SIN nanomembrane and deionized ultrapure water was observed using 30 frames/s imaging. The EB was irradiated at 2.5 keV with beam current of 0.67–2.0 nA and at 5 keV with beam current of 0.9 nA. These profiles of luminescence intensity were processed using Image J (NIH).

Behavior of the EB-induced deposition in an aqueous solution was observed using 100 frames/s in 10 mM 3,4-ethylenedioxythiophene (EDOT; 483028, Sigma–Aldrich) solution diluted in deionized ultrapure water. The 2.5 keV EB with beam current of 34 nA was irradiated during rectangular raster scanning (2.8 μm × 2.1 μm) on the SiN nanomembrane. The current intensity in the scanning area was 5.8 nA μm^{-2}. Reflecting images were captured under the incident white light from the LED light source.

2.4. In situ patterning on a culturing cell

Hep G2 cells (Human hepatocellular liver carcinoma cell line, RCB1648, Riken cell bank) were cultured in minimum essential medium containing 10% fetal bovine serum and 0.1 mM non-essential amino acids. Hep G2 cells were seeded on the SiN nanomembrane and incubated at 37 °C with 5% in the humidified incubator for a few days. The SiN nanomembrane with cells in it was placed in the EB setup. The EB was irradiated at 2.5 keV with rectangular raster scanning to a cell. The center of the cell was targeted using real-time imaging of the sCMOS camera. The culture medium was heated at 35–37 °C using a lens heater attached on the water immersion objective lens.

3. Results

3.1. Simulated energy profile

The Monte Carlo simulation showed that the SiN nanomembrane transmitted the electron kinetic energy of the 2.5 keV EB to the opposite side of the 100-nm-thick nanomembrane

(Fig. 1B). Although most of the primary electrons were scattered in the lateral range of a few hundred nanometers at the SiN membrane, only a few transmitted electrons entered the H_2O layers in the lateral range of about a hundred nanometers. An energy distribution graph of the relative number transmitted electrons according to transmission energy at the interface between SiN and H_2O indicated that the transmission energy was limited below about 1 keV at an irradiation beam energy around 2.5 keV (Fig. 2A). This remaining kinetic energy of the transmitted electrons was absorbed by the H_2O. Absorbed energy density at the SiN/H_2O interface was plotted as a function of the lateral profile in Fig. 2(B). Though the simulated profile of absorbed energy density depended on the initial irradiation energy of the EB, absorbed energy density was below 10^{-2} eV nm^{-3}. At 2.5 keV and 5 keV beam irradiations, the absorbed energy density had full width at half maximum (FWHM) values of 50 nm and 25 nm, respectively.

3.2. Profile of electron beam-induced luminescence

The sCMOS camera could detect the luminescent light spot in the video images in real-time. A supplemental video (Supplementary Movie01.wmv) shows a continuously moving light spot which was induced by 2.5 keV EB scanning. The trajectory was plotted in Fig. 2(E). Fig. 2(C) and (D) showed intensity profiles of the light spot at 2.5 keV and 5 keV. The intensity of the light spot increased as a function of accelerating voltage of the EB and its beam current. FWHM values of the profile of electron beam-induced luminescence were 473 nm and 266 nm at 2.5 keV and 5 keV, respectively.

3.3. Real-time observation of deposition

In the EDOT solution, raster scanning induced deposition of a rectangular micro pattern on the SiN nanomembrane. Real-time observation using the sCMOS camera is shown in a supplemental video (Supplementary Movie2.wmv). The pattern gradually appeared as a visible convex texture during the EB scanning. Fig. 3 summarizes time series behavior of the brightness profiles for the depositing video (Supplementary Movie2.wmv). The increasing brightness of the deposition pattern in the video images indicated interference of reflected light at the growing thin film during the EB scanning. In this process, the right edge was brighter than other areas including the left edge (Fig. 3A).

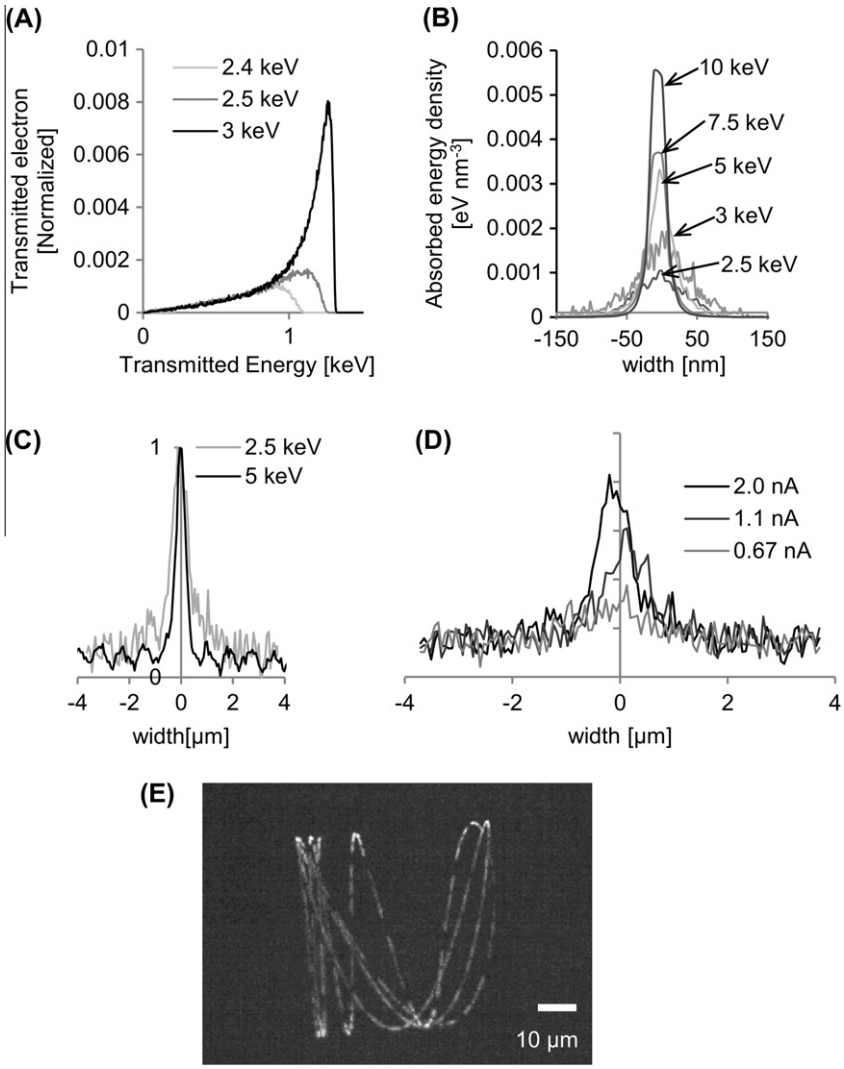

Fig. 2. Energy profile of electrons transmitted through the 100-nm-thick SIN nanomembrane. (A) Energy distributions of transmitted primary electrons by Monte Carlo simulation. The energy distributions were normalized with the initial number of primary electrons. (B) Simulated absorbed energy of the spot profile at the interface between the SiN nanomembrane and water. (C) Intensity profiles of the light spot at 2.5 keV and 5 keV. The peaks of the profiles were normalized. (D) Intensity profiles of the light spot at 2.5 keV with various beam current. (E) Sequence photographs of electron-induced luminescence at the 100-nm-thick SiN layer with multiple exposures at 40-ms intervals. The input beam trajectory was the Lissajous diagram. (D) Profiles of the EB-induced luminescence.

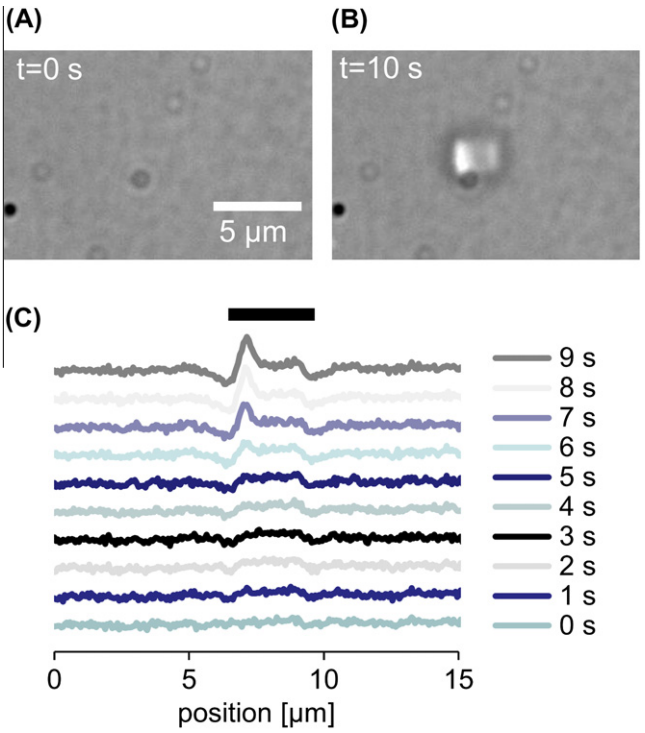

Fig. 3. EB-induced deposition of EDOT at the interface of the 100-nm-thick SiN nanomembrane and the 10 mM EDOT solution in water. (A and B) Rectangular deposition patterns from the video (SupplMovie2.wmv) images. (C) Time sequence of the brightness profiles of the video images during processing of the rectangular deposition. The white bar in (A) indicates the width of the EB scanning pattern.

3.4. In situ patterning on a Hep G2 cell

The EB was aligned to the center of the camera view using both the secondary electron image and EB-induced luminescence spot light. Then the target Hep G2 cell was aligned to the center of the view window of the sCMOS camera Therefore the processing area could be precisely controlled to the targeted point on the cell which was scanned with a rectangular raster pattern. Fig. 4 shows the EB-induced patterning on the cell center.

4. Discussion

Our Monte Carlo simulation showed a few primary electrons reached the SiN/H_2O interface, and those few transmitted electrons had kinetic energy of less than about 1 keV. We purposely used a low energy EB to reduce damage to the bio-molecules during the beam irradiation. These simulation results indicated even low energy electrons could reach the SiN/H_2O interface and their lateral scattering region (<50 nm) was similar in size to a composite bio-molecule. This kinetic energy of transmitted electrons could contribute to chemical reactions at the SiN/H_2O interface due to energy absorption by H_2O. The extremely small absorbed energy was smaller than the thermal energy at room temperature (~1/40 eV). Therefore, the primary electrons would not be the dominant factor for chemical reaction changes in the solution or for inducing bio-molecular damages, because molecular bond energies are on the order of 1 eV per molecule. Secondary electrons, which were produced around scattering trajectories of scattering primary electrons and generally with energies <20 eV, would be the dominant factor for the EB-induced reaction. The EB induces a surface chemical reaction to deposit precursor materials due to emission of scattering, back scattering and also secondary electrons from the surface [13,14]. These low energy electrons have enough energy to ionize atomic hydrogen (13.6 eV). Though these energies are sufficient to generate single strand breaks of DNA samples in a biological application, they fortunately do not induce the critical double strand breaks for DNA molecules which are less repairable in correction process [15,16].

The reactive region induced by the EB was visualized using luminescence video images at the SiN/H_2O interface. The FWHM values of the luminescence light spot were related to acceleration voltage and beam current of the irradiating EB. These sizes were 10 times larger than the simulated results of scattering primary electrons. This difference indicated the luminescence region was not related to only primary electrons but also secondary electrons around the primary electrons, and the captured image showed the diffraction pattern of a point source. Such 10-fold enlargement of the processing area was previously reported in the case of chemical vapor deposition using an electron (or ion) beam as a result of secondary electron-induced surface reactions [17]. The intensity profile of the light spot (Fig. 2C) included typical periodic rises like those of a high order diffraction pattern in Fig. 2C. Diffraction limit of the objective lens on the optical microscope was calculated as 277 nm at 500 nm wavelength light. The reactive region induced by the EB would be less than the diffracted image of the luminescence; therefore the resolution would be less than the diffraction limit of a conventional focused laser processing using an optical objective lens.

Synchronizing imaging of the EB-induced processing could be visualized using the real-time observation and *in situ* processing in the nanometer-scale world of the cell culturing environment.

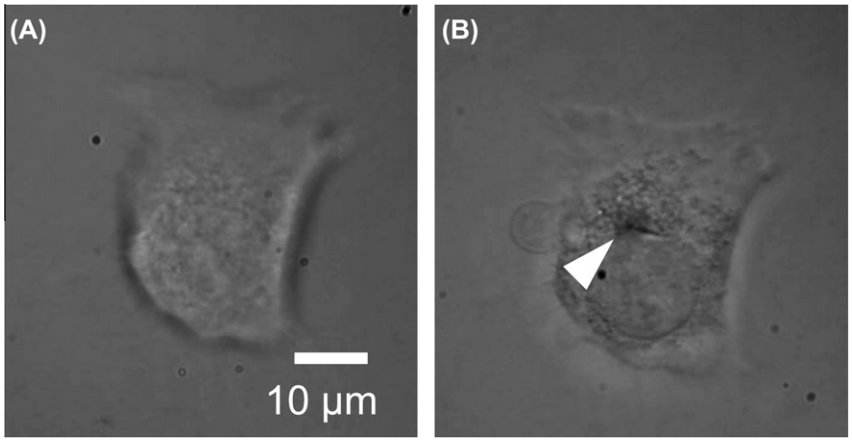

Fig. 4. *In situ* EB-induced patterning on a culturing hepatocyte cell. (A) A Hep G2 hepatocyte cell which was culturing on the SiN nanomembrane was targeted using a real-time live image from the sCMOS camera. (B) The electron beam was scanned at the center of the cell.

Real-time observation contributed to achieving precise alignment for the calibration procedure which overlapped the optical image and the EB scanning route. The peak intensity of the light spot of luminescence could be detected within a few tens of nanometers. Thus, we successfully demonstrated the *in situ* processing on the center of the culturing cell. And we also characterized the basic processing behavior in spatio-temporal changes using video data. The deposited rectangular EDOT pattern was somewhat uneven in the rectangular scanning area. The left edge of the deposited pattern was a ridge and higher than other flat areas. This asymmetric deposition would result from hysteresis of the polymerization process and signals of the pattern generator. Raster scanning was started from the left and moved toward the right of the rectangular pattern; therefore the left edge retained a higher reactive energy and molecular concentration than the right edge. Similar phenomena showing scanning direction-dependent deposition were reported previously in research studies on chemical vapor deposition using a focused ion beam [18]. This hysteresis effect could be reduced by controlling the dwell time for the beam scanning pattern using high speed blanking of the electron beam.

The EB induced a surface chemical reaction to deposit liquid precursor materials due to emission of secondary electrons from the surface at the culturing cell. This was a result of the energy of the secondary electrons being equivalent to the energy of a redox reaction. The EB-induced chemical reaction could be applied to modification of the cell membrane traffic as nano stimulation probes. Previously, we reported no damage on a living cell membrane after deposition of a precursor material 3,4-ethylenedioxythiophene using a low energy EB irradiation through a thin nanomembrane in a wet SEM capsule [10]. Less damage and *in situ* processing on the living cell might be possible using a nano stimulator and nano manipulation for living molecular and cell systems. This would mean the molecule resolution computational environment was virtually displayed for living cells using EB scanning. The reactive energy range could be chosen based on the accelerating voltage and beam current of the EB and the spatio-temporal scanning pattern.

In summary, we described our use of EB lithography and an optical microscope that was connected in a closed-loop to synchronize beam irradiation and camera views for *in situ* nano processing. The opposed co-axial dual optics including an I-EBL system and an optical microscope could provide *in situ* nano processing of a culturing living cell on a 100-nm-thick SiN nanomembrane. Imaging synchronized to the I-EBL and real-time observation during the EB irradiation visualized dynamics of the EB-induced deposition and nano processing of the living cell. Resolution of less than a few hundred nanometers was visualized in real-time by the high sensitivity camera mounted on the optical microscope. The closed-looped *in situ* nano processing should be a good tool for nano biological research studies. The applicability of the nano processing should be widespread owing to the high resolution and controllability of the beam scanning and we expect it to be used for nanometer resolution displays of virtual molecule environments to study functional changes of biomolecule systems.

Acknowledgments

The present work was supported in part by Grants-in-Aid for Scientific Research from The Ministry of Education, Culture, Sports, Science and Technology in Japan Nos. 23680052 and 23656179, and The Ring Ring Project of the JKA Foundation.

Appendix A. Supplementary data

Supplementary data associated with this article can be found, in the online version, at http://dx.doi.org/10.1016/j.bbrc.2013.01.100.

References

[1] A. Pimpin, W. Srituravanich, Review on micro- and nanolithography techniques and their applications, Eng. J. 16 (2012) 37–56.
[2] H. Minoda, T. Okabe, Y. Inayoshi, T. Miyakawa, Y. Miyauchi, M. Tanokura, et al., Electron microscopic evidence for the myosin head lever arm mechanism in hydrated myosin filaments using the gas environmental chamber, Biochem. Biophys. Res. Commun. 405 (2011) 651–656.
[3] H. Sugi, H. Minoda, Y. Inayoshi, F. Yumoto, T. Miyakawa, Y. Miyauchi, et al., Direct demonstration of the cross-bridge recovery stroke in muscle thick filaments in aqueous solution by using the hydration chamber, Proc. Natl. Acad. Sci. USA 105 (2008) 17396–17401.
[4] T. Ogura, Direct observation of unstained wet biological samples by scanning-electron generation X-ray microscopy, Biochem. Biophys. Res. Commun. 391 (2010) 198–202.
[5] I. Motoyoshi, S. Nishida, L. Sharan, E.H. Adelson, Image statistics and the perception of surface qualities, Nature 447 (2007) 206–209.
[6] C. Sato, S. Manaka, D. Nakane, H. Nishiyama, M. Suga, T. Nishizaka, et al., Rapid imaging of mycoplasma in solution using atmospheric scanning electron microscopy (ASEM), Biochem. Biophys. Res. Commun. 417 (2012) 1213–1218.
[7] W. Inami, K. Nakajima, A. Miyakawa, Y. Kawata, Electron beam excitation assisted optical microscope with ultra-high resolution, Opt. Express 18 (2010) 12897–12902.
[8] Y. Nawa, W. Inami, A. Chiba, A. Ono, A. Miyakawa, Y. Kawata, et al., Dynamic and high-resolution live cell imaging by direct electron beam excitation, Opt. Express 20 (2012) 5629.
[9] E.U. Donev, J.T. Hastings, Electron-beam-induced deposition of platinum from a liquid precursor, Nano Lett. 9 (2009) 2715–2718.
[10] T. Hoshino, K. Morishima, Electron-beam direct processing on living cell membrane, Appl. Phys. Lett. 99 (2011) 174102.
[11] T. Hoshino, K. Morishima, Electron-beam induced *in situ* spatiotemporal nanofabrication toward intracellular nanorobotics, in: Proc. The 14th International Conference on Miniaturized Systems for Chemistry and Life Science (μTAS), 2010, p. W63A.
[12] D. Drouin, A.R. Couture, D. Joly, X. Tastet, V. Aimez, R. Gauvin, CASINO V2.42 – a fast and easy-to-use modeling tool for scanning electron microscopy and microanalysis users, Scanning 29 (2007) 92–101.
[13] H.W.P. Koops, R. Weiel, D.P. Kern, T.H. Baum, High resolution electron beam induced deposition, J. Vac. Sci. Technol., B 6 (1988) 477–481.
[14] J.D. Fowlkes, S.J. Randolph, P.D. Rack, Growth and simulation of high-aspect ratio nanopillars by primary and secondary electron-induced deposition, J. Vac. Sci. Technol., B 23 (2005) 2825–2832.
[15] B. Boudaiffa, P. Cloutier, D. Hunting, M.A. Huels, L. Sanche, Resonant formation of DNA strand breaks by low-energy (3 to 20 eV) electrons, Science 287 (2000) 1658–1660.
[16] A. Joubert, N. Foray, Repair of radiation-induced DNA double-strand breaks in human cells: History, Progress and Controversies, in: B.R. Landseer (Eds.), New Research on DNA Repair, Nova Science Publishers Inc., New York, 2007, pp. 273–294.
[17] J. Fujita, M. Ishida, T. Ichihashi, Y. Ochiai, T. Kaito, S. Matsui, Carbon nanopillar laterally grown with electron beam-induced chemical vapor deposition, J. Vac. Sci. Technol., B 21 (2003) 2990.
[18] T. Hoshino, K. Watanabe, R. Kometani, T. Morita, K. Kanda, Y. Haruyama, et al., Development of three-dimensional pattern-generating system for focused-ion-beam chemical-vapor deposition, J. Vac. Sci. Technol., B 21 (2003) 2732–2736.